Article

Dynamics in a Pure Encounter Complex of Two Proteins Studied by Solution Scattering and Paramagnetic NMR Spectroscopy

Xingfu Xu, Wolfgang Reinle, Frank Hannemann, Peter V. Konarev, Dmitri I. Svergun, Rita Bernhardt, and Marcellus Ubbink

J. Am. Chem. Soc., **2008**, 130 (20), 6395-6403 • DOI: 10.1021/ja7101357 • Publication Date (Web): 26 April 2008

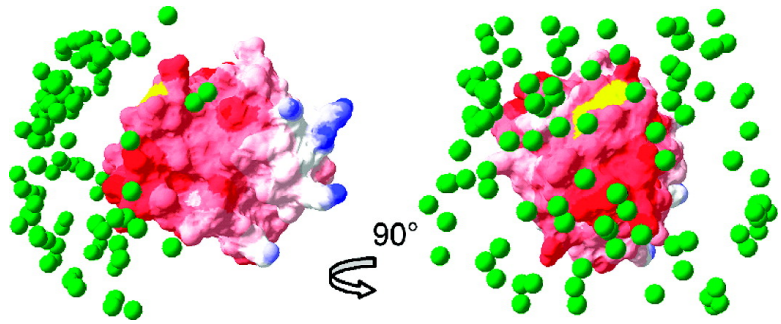

J|A|C|S
ARTICLES

Published on Web 04/26/2008

Dynamics in a Pure Encounter Complex of Two Proteins Studied by Solution Scattering and Paramagnetic NMR Spectroscopy

Xingfu Xu,[†] Wolfgang Reinle,[‡] Frank Hannemann,[‡] Peter V. Konarev,[§,||] Dmitri I. Svergun,[§,||] Rita Bernhardt,[‡] and Marcellus Ubbink*,[†]

Institute of Chemistry, Leiden University, P.O. Box 9502, NL-2300RA Leiden, The Netherlands, Naturwissenschaftlich-Technische Fakultat III, Institut für Biochemie, Universität des Saarlandes, P.O. Box 151150, D-66041, Saarbrucken, Germany, EMBL Hamburg, Notkestrasse 85, D-22603 Hamburg, Germany, and Institute of Crystallography, Russian Academy of Sciences, Leninsky pr. 59, 117333, Moscow, Russia

Received November 8, 2007; E-mail: m.ubbink@chem.leidenuniv.nl

Abstract: In the general view of protein-complex formation, a transient and dynamic encounter complex proceeds to form a more stable, well-defined, and active form. In weak protein complexes, however, the encounter state can represent a significant population of the complex. The redox proteins adrenodoxin (Adx) and cytochrome *c* (C*c*) associate to form such a weak and short-lived complex, which is nevertheless active in electron transfer. To study the conformational freedom within the protein complex, the native complex has been compared to a cross-linked counterpart by using solution scattering and NMR spectroscopy. Oligomerization behavior of the native complex in solution revealed by small-angle X-ray scattering indicates a stochastic nature of complex formation. For the cross-linked complex, interprotein paramagnetic effects are observed, whereas for the native complex, extensive averaging occurs, consistent with multiple orientations of the proteins within the complex. Simulations show that C*c* samples about half of the surface area of adrenodoxin. It is concluded that the complex of Adx/C*c* is entirely dynamic and can be considered as a pure encounter complex.

Introduction

The formation of a protein complex is at least a two-step process, in which a dynamic encounter complex precedes the final, well-defined complex. It has been proposed that the role of the former is to enable a reduced-dimensionality search of the optimal binding geometry, thus accelerating molecular association.[1] Generally, it is assumed that the encounter state exists only briefly and leads quickly to the well-defined, final complex. However, analysis by NMR spectroscopy has suggested that for weak protein complexes, the encounter state represents a significant fraction of the population or can even be the dominant form. This was concluded from the observation that for these complexes, the average chemical-shift perturbations (CSPs) observed upon complex formation are very small, and the residues involved are spread over a large part of the protein surface.[2,3] This view is in line with the conclusions of independent studies on the electron-transfer (ET) rates in ET complexes.[4,5] Recently, the encounter state was visualized by a paramagnetic NMR technique for complexes in which it represents a small fraction of the population.[6,7] In weak protein complexes, the fraction of time spent in the encounter complex may be the largest because a balance between specificity and fast dissociation has to be found.

To study the elusive encounter state and obtain more direct evidence of its dynamic nature, we decided to compare an ET complex in its native form with a cross-linked (CL) complex of the same proteins. Adrenodoxin (Adx) is a 14.4 kDa protein that belongs to the family of vertebrate-type 2Fe-2S ferredoxin. It is involved in steroid hormone biosynthesis by acting as an electron shuttle between NADPH-dependent Adx reductase and several cytochromes P450.[8] In vitro ET from Adx reductase to Adx is often monitored by fast subsequent ET from Adx to mitochondrial cytochrome *c* (C*c*). C*c* serves in the reaction as a model for cytochrome P450.[9] The interaction of yeast C*c* with full-length bovine Adx and truncated Adx4-108 has been studied

[†] Leiden University.
[‡] Universität des Saarlandes.
[§] EMBL Hamburg.
[||] Russian Academy of Sciences.

(1) Delbrück M.; Adam G. Reduction of Dimensionality Biological Diffusion Processes. In *Structural Chemistry and Molecular Biology*; Rich A., Davidson N., Eds.; Freeman: San Francisco, 1968; pp 198−215..
(2) Ubbink, M.; Bendall, D. S. *Biochemistry* **1997**, *36*, 6326–6335.
(3) Worrall, J. A. R.; Reinle, W.; Bernhardt, R.; Ubbink, M. *Biochemistry* **2003**, *42*, 7068–7076.
(4) Hoffman, B. M.; Celis, L. M.; Cull, D. A.; Patel, A. D.; Seifert, J. L.; Wheeler, K. E.; Wang, J. Y.; Yao, J.; Kurnikov, I. V.; Nocek, J. M. *Proc. Natl. Acad. Sci.U.S.A.* **2005**, *102*, 3564–3569.
(5) Liang, Z. X.; Kurnikov, I. V.; Nocek, J. M.; Mauk, A. G.; Beratan, D. N.; Hoffman, B. M. *J. Am. Chem. Soc.* **2004**, *126*, 2785–2798.
(6) Tang, C.; Iwahara, J.; Clore, G. M. *Nature* **2006**, *444*, 383–386.
(7) Volkov, A. N.; Worrall, J. A. R.; Holtzmann, E.; Ubbink, M. *Proc. Natl. Acad. Sci.U.S.A.* **2006**, *103*, 18945–18950.
(8) Grinberg, A. V.; Hannemann, F.; Schiffler, B.; Müller, J.; Heinemann, U.; Bernhardt, R. *Proteins: Struct., Funct., Genet.* **2000**, *40*, 590–612.
(9) Lambeth, J. D.; Kamin, H. *J. Biol. Chem.* **1979**, *254*, 2766–2774.

by NMR spectroscopy.[3] It was shown that a complex is formed despite the fact that the proteins are nonphysiological partners. The dissociation constant is 25 μM in 20 mM potassium phosphate buffer, which is in the range of other ET complexes.[10] Chemical-shift mapping indicated that an extensive interface exists in this complex, especially on the Adx part. The results suggested that this complex is a dynamic ensemble of orientations with both proteins sampling other surface areas, away from the predominant binding sites. Thus, the complex potentially represents a good model to study the characteristics of encounter complex. The FeS cluster in Adx and the heme in C*c* can serve as natural paramagnetic centers to probe the averaging effects within the complex.

In this study, a CL complex was constructed with an engineered intermolecular disulfide bond to serve as a rigid control complex. Small-angle X-ray scattering (SAXS) reveals an oligomerization behavior different for the CL and native complexes, which is consistent with dynamic complex formation. It is shown that for the rigid complex, large CSPs and significant intermolecular paramagnetic effects can be detected, in contrast with the native complex. These differences are explained by averaging effects due to multiple orientations of two proteins in the native complex. Simulations suggest that in the native complex, averaging over a surprisingly large interaction interface is required to reduce the paramagnetic effects to insignificant values, which is consistent with the observations from NMR chemical-shift mapping. The results indicate that this complex is entirely dynamic and can be interpreted as a pure encounter complex.

Materials and Methods

Site-Directed Mutagenesis Experiment and Protein Production. Site-directed mutagenesis was performed by using the QuikChange method (Stratagene, La Jolla, CA). Two mutants, yeast C*c*V28C and the double mutant L80C/C95S of truncated, bovine Adx (residues 4−108),[11] were constructed. The C95S mutation removes a native semi-exposed Cys. Mutations were confirmed by DNA sequencing.

Production and purification of wild-type (WT) and mutant C*c* were performed as reported.[12] For ^{15}N-enriched C*c*V28C, the production conditions were optimized to improve the yield (see Supporting Information). The production and expression of Adx mutant was performed as reported[3] and purified by using a Source-30Q anion exchange column and a Superdex G75 gel filtration column.

Cross-Linking. C*c*V28C and AdxL80C were treated with 5 mM DTT in 50 mM sodium phosphate buffer, pH 6.5, with 500 mM Na_2SO_4. After 1 h, the buffer was changed to 50 mM Tris, pH 8.0, containing 500 mM Na_2SO_4 by using ultrafiltration on a 3 kDa cutoff membrane. Both proteins were diluted to 200 μM and mixed, and $K_3Fe(CN)_6$ was added to the final concentration of 5 mM to oxidize the mixture.

The covalent complex was purified from the C*c*V28C and AdxL80C monomers and homodimers by ion-exchange chromatography. The buffer of the oxidized mixture was changed to 50 mM Tris, pH 8.0, and a small amount of ascorbic acid was added to reduce the C*c* of the heterodimer before the mixture was loaded to a MonoQ column attached to an ÄKTA FPLC system (GE Healthcare Inc., Benelux).

The C*c*V28C monomer and homodimer were found in the flow-through. The heterodimer was eluted with a salt gradient ranging from 150 mM to 200 mM NaCl, whereas AdxL80C was not eluted until the salt concentration was increased to 400 mM.

The CL heterodimer was characterized on an analytical Superdex G75 10/300 GL gel filtration column by using a solution containing 25 mM sodium phosphate, pH 7.4.

SAXS. The synchrotron radiation X-ray scattering data were collected on the X33 camera of the EMBL (DESY, Hamburg, Germany)[13] and analyzed according to standard procedures.[14] Solutions of native and CL complex of C*c* and Adx were measured at 15 °C in solute concentration range from 2.4 to 24.0 mg/mL in 10 mM Hepes, pH 7.4 buffers, with 0, 40, 80, 120, 200, and 300 mM NaCl. The solutions of native complex of solute range from 2.4 to 7.2 mg/mL in 20 mM potassium phosphate buffer were also measured to check the oligomerization status. The data were recorded by using a MAR345 two-dimensional image plate detector at a sample−detector distance of 2.7 m and a wavelength of λ = 1.5 Å, covering the range of momentum transfer $0.012 < s < 0.45$ Å^{-1} ($s = (4\pi \sin\theta)/\lambda$, where 2θ is the scattering angle). All data manipulations were performed by using the program package PRIMUS.[15] The forward scattering $I(0)$ and the radius of gyration (R_g) were evaluated by using the Guinier approximation assuming that at very small angles ($s < 1.3/R_g$), the intensity is represented as $I(s) = I(0) \exp(-(sR_g)^2/3)$. These parameters and the maximum diameter D_{max} of the particle were also computed from the entire scattering patterns by using the program GNOM.[16] The excluded volume V_p of the particle was computed from the Porod invariant.[17] The molecular masses of the solutes were evaluated by comparison of the forward scattering with that from reference solutions of bovine serum albumin (MM = 66 kDa). The low resolution shapes were reconstructed ab initio by DAMMIN,[18] the scattering from the high-resolution models was computed by CRYSOL,[19] and the volume fractions of oligomers were determined by OLIGOMER.[15]

The structure of the C*c*/Adx CL complex was refined by rigid body modeling by using the program SASREF.[20] The latter program employs a simulated annealing protocol to generate an interconnected assembly of subunits without steric clashes fitting the scattering data. Contact information on the residues involved in the dimerization was included as a restraint. The scattering amplitudes from the crystallographic models of C*c* (PDB 2YCC)[21] and Adx (PDB 1AYF)[22] were calculated by using the program CRYSOL.[19]

For a quantitative description C*c*/Adx native complex at different protein and NaCl concentrations, the experimental intensity $I_{exp}(s)$ was represented by linear combinations of the curves computed from putative complexes at different stoichiometry. Given the scattering curves of such components, the program OLIGOMER[15] finds the volume fractions by solving a system of linear equations to minimize discrepancy between the experimental and calculated scattering curves.

(10) Crowley, P. B.; Ubbink, M. *Acc. Chem. Res.* **2003**, *36*, 723–730.
(11) Uhlmann, H.; Kraft, R.; Bernhardt, R. *J. Biol. Chem.* **1994**, *269*, 22557–22564.
(12) Rumbley, J. N.; Hoang, L.; Englander, S. W. *Biochemistry* **2002**, *41*, 13894–13901.
(13) Roessle, M. W.; Klaering, R.; Ristau, U.; Robrahn, B.; Jahn, D.; Gehrmann, T.; Konarev, P.; Round, A.; Fiedler, S.; Hermes, C.; Svergun, D. *J. Appl. Crystallogr.* **2007**, *40*, S190–S194.
(14) Konarev, P. V.; Petoukhov, M. V.; Volkov, V. V.; Svergun, D. I. *J. Appl. Crystallogr.* **2006**, *39*, 277–286.
(15) Konarev, P. V.; Volkov, V. V.; Sokolova, A. V.; Koch, M. H. J.; Svergun, D. I. *J. Appl. Crystallogr.* **2003**, *36*, 1277–1282.
(16) Svergun, D. I. *J. Appl. Crystallogr.* **1992**, *25*, 495–503.
(17) Porod, G. In *General Theory. Small-Angle X-ray Scattering*; Glatter, O., Kratky, O., Eds.; Academic Press: London, 1982; pp 17−51.
(18) Svergun, D. I. *Biophys. J.* **1999**, *77*, 2896.
(19) Svergun, D.; Barberato, C.; Koch, M. H. J. *J. Appl. Crystallogr.* **1995**, *28*, 768–773.
(20) Petoukhov, M. V.; Svergun, D. I. *Biophys. J.* **2005**, *89*, 1237–1250.
(21) Berghuis, A. M.; Brayer, G. D. *J. Mol. Biol.* **1992**, *223*, 959–976.
(22) Müller, A.; Müller, J. J.; Müller, Y. A.; Uhlman, H.; Bernhard, R.; Heineman, U. *Structure* **1998**, *6*, 269–280.

$$\chi^2 = \frac{1}{N-1}\sum_j \left[\frac{I(s_j) - cI_{calc}(s_j)}{\sigma(s_j)}\right]^2 \quad (1)$$

where N is the number of experimental points, c is a scaling factor, and $I_{calc}(s)$ and $\sigma(s_j)$ are the calculated intensity and the experimental error at the momentum transfer s_j, respectively. The possible components included individual proteins (monomers), 1:1 cytochrome/Adx complex (dimer), and tentative higher oligomeric models, 2:1 and 1:2 complexes (trimers) and 2:2 complexes (tetramers).

NMR Experiments. NMR experiments were performed in 20 mM phosphate buffers, pH 7.4, consistent with earlier work. In this buffer, no indications for oligomerization of the complex were observed on the basis of the absence of concentration-dependent line broadening effects. In 10 mM Hepes, pH 7.4, the NMR spectra of the complex exhibited very broad line width, consistent with trimer and tetramer formation as observed in the SAXS experiments. Samples contained 0.2−1 mM (for assignment) protein, 5% D_2O. For backbone assignment of CL complex, 0.4 M Na_2SO_4 was present in the buffer. Protein concentrations were determined by using $\epsilon_{410} = 106$ $mM^{-1}cm^{-1}$ for ferric C*c*, $\epsilon_{550} = 27.5$ $mM^{-1}cm^{-1}$ for ferrous C*c*, $\epsilon_{414} = 9.8$ $mM^{-1}cm^{-1}$ for oxidized Adx, and $\epsilon_{550} = 31.7$ $mM^{-1}cm^{-1}$for the reduced CL heterodimer.

All NMR experiments were carried out on a Bruker DMX 600 spectrometer equipped with a TXI-Z-GRAD probe or a TCI-Z-GRAD cryoprobe. For ^{15}N-labeled C*c*V28C, the assignment of backbone amide resonances was based on WT C*c*[23] and confirmed by the analysis of an ^{15}N NOESY-HSQC spectrum. The backbone amide assignment of AdxL80C was completed with ^{15}N TOCSY-HSQC and NOESY-HSQC spectra based on previous assignments for Adx.[3] For the CL heterodimer, a ^{15}N NOESY-HSQC spectrum was recorded at a temperature of 301 K. The backbone amide assignments were confirmed by the analysis of NOE connectivities. Processing was performed by using AZARA (http://bio.cam.ac.uk/azara) and the spectra were analyzed in Ansig-for-Windows.[24] The averaged amide CSP ($\Delta\delta_{avg}$) was derived from

$$\Delta\delta_{avg} = \sqrt{\frac{(\Delta\delta N/5)^2 + \Delta\delta H^2}{2}} \quad (2)$$

where $\Delta\delta$N and $\Delta\delta$H represent the chemical-shift change for the amide nitrogen and proton, respectively.

Pseudocontact Shift (PCS) Measurements and R_1 Relaxation-Rate Measurements. For free C*c*V28C, the chemical-shift difference between ferric and ferrous C*c* was taken to represent the PCS. To detect PCS in the native complex, two HSQC spectra were recorded for ^{15}N Adx (0.2 mM) in the presence of ferric or ferrous C*c* in a ratio 1:2.5. For the CL complex, four samples were prepared, with either C*c* or Adx labeled with ^{15}N and with C*c* either reduced or oxidized. Thus, PCS could be measured for both C*c* and Adx within the complex. Magnetic susceptibility tensors were calculated according to Worrall et al.[23] The tensor size and orientation are identical within error for free C*c* and the CL heterodimer and similar to those reported,[23] see Supporting Information Table S1 and Figure S1.

The longitudinal relaxation rates of the amide protons of C*c* in the free state and the native and CL complex were obtained by a series of inversion−recovery (IR) ^{1}H−^{15}N HSQC spectra. Water suppression was achieved by presaturation. The IR relaxation delays (τ) were 0.001, 0.01, 0.03, 0.05, 0.1, 0.2, 0.35, 0.55, 0.85, 1.4, and 3.0 s. The spectra were acquired in an interleaved way, such that all delays were applied before incrementing the indirect dimension. The amide proton R_1 relaxation rates were obtained by a three-parameter single-exponential fit of the HSQC crosspeak intensities $I(\tau)$ by using

$$I(\tau) = I_{eq} - (I_{eq} - I_0)\exp(-R_1\tau) \quad (3)$$

where I_0 is the magnetization at time $\tau = 0$ s and I_{eq} is the equilibrium magnetization. $I(\tau)$ and τ are the dependent and independent variables, respectively, and I_0, I_{eq}, and R_1 are the fitted parameters.

Site-Specific Spin Labeling. C*c*V28C was incubated with 10 mM DTT in 0.1 M Tris·HCl (pH 8.0)/0.1 M NaCl for 2 h at room temperature to reduce intermolecular disulfide bonds. DTT was removed by passing the protein solution through a PD-10 column (Amersham Pharmacia, Uppsala, Sweden). The resulting monomeric protein was reacted with 10-fold excess of paramagnetic label, 1-oxyl-2,2,5,5-tetramethyl-3-pyrroline-3-methyl)-methanethiosulfonate (MTSL), or diamagnetic control label, 1-acetyl-2,2,5,5-tetramethyl-3-pyrroline-3-methyl)-methanethiosulfonate (MTS), and incubated overnight at room temperature. MTSL and MTS were purchased from Toronto Research Chemicals (North York, ON, Canada) and used without further purification. Upon completion of the reaction, the solution was passed through a PD-10 column to remove any unreacted label, and the buffer was changed by ultrafiltration. The yield of labeling was about 90% as estimated from double-integrated electron paramagnetic resonance spectra of C*c*-MTSL and a control sample containing a known amount of free MTSL. Samples of ^{15}N Adx complexed with either C*c*V28C-MTSL (1:2.5) or C*c*V28C-MTS were prepared in a parallel way. Both samples contained the same amount of ^{15}N acetemide as an internal reference. HSQC spectra were measured for both samples, and the attenuation factor was determined by taking the ratio of heights of crosspeaks observed for amide resonances of Adx for both samples (I_{para}/I_{dia}). The paramagnetic relaxation enhancement (PRE, $R_{2,para}$) was calculated from the following equation:

$$\frac{I_{para}}{I_{dia}} = \frac{R_{2,dia}\exp(-tR_{2,dia})}{R_{2,dia} + R_{2,para}} \quad (4)$$

where t is the INEPT evolution time of HSQC (9 ms), and $R_{2,dia}$, the diamagnetic transverse relaxation rate, was obtained from the line width of the HSQC crosspeaks of the ^{15}N Adx in the complex with C*c*V28C-MTS, according to the reported method.[25]

To exclude the possible contribution of PRE due to the nonspecific interaction between MTSL nitroxide group with Adx, we also estimated the PRE effect caused by several concentrations of free nitoxide spin label TEMPOL. Only at very high concentration of free spin label TEMPOL (>10 mM), a general broadening effect is found for Adx (Supporting Information, Figure S2 and S3), which is consistent with previous studies.[26,27] At 0.5 mM, the concentration of labeled protein used in our experiments, PRE contributions due to nonspecific interactions are <5 s^{-1}.

Structure Calculation of the CL Complex. The structure coordinates were taken from Protein Data Bank (PDB), entries 1YCC[28] for C*c* and 1AYF for Adx.[22] The mutations were introduced in Swiss-PDB viewer.[29] The protein structure coordinates were linked together through a disulfide bond formed by C28 of C*c* and C80 of Adx in XPLOR-NIH.[30] By consecutive rotation of the five torsion angles between C*c*V28C C_α and AdxL80C C_α in steps of 10°, the conformation space was sampled systematically, and the rotamers were scored on the basis of van der Waals, PCS, and PRE energy terms. The tensor and the 20 intermolecular PCS observed for Adx were used as input in the structure calculations.

(23) Worrall, J. A. R.; Kolczak, U.; Canters, G. W.; Ubbink, M. *Biochemistry* **2001**, *40*, 7069–7076.
(24) Helgstrand, M.; Kraulis, P.; Allard, P.; Härd, T. *J. Biomol. NMR* **2000**, *18*, 329–336.
(25) Vlasie, M. D.; Fernández-Busnadiego, R.; Prudêncio, M.; Ubbink, M. *J. Mol. Biol.* **2008**, *375*, 1405–1415.
(26) Niccolai, N.; Spiga, O.; Bernini, A.; Scarselli, M.; Ciutti, A.; Fiaschi, I.; Chiellini, S.; Molinari, H.; Temussi, P. A. *J. Mol. Biol.* **2003**, *332*, 437–447.
(27) Deschamps, M. L.; Pilka, E. S.; Potts, J. R.; Campbell, I. D.; Boyd, J. *J. Biomol. NMR* **2005**, *31*, 155–160.
(28) Louie, G. V.; Brayer, G. D. *J. Mol. Biol.* **1990**, *214*, 527–555.
(29) Guex, N.; Peitsch, M. C. *Electrophoresis* **1997**, *18*, 2714–2723.
(30) Schwieters, C. D.; Kuszewski, J. J.; Tjandra, N.; Clore, G. M. *J. Magn. Reson.* **2003**, *160*, 65–73.

Table 1. Parameters of Native Cytochrome−Adx Complex from SAXS Data[a]

	native complex, in 10 mM Hepes, pH 7.4				CL complex	*Cc*/Adx (NMR)
c (mg/mL)	24	12	6	2.4	3−12	
R_g (Å)	28.3 ± 0.7	28.3 ± 0.7	26.5 ± 0.5	24.4 ± 0.7	21.4 ± 0.5	20.4
D_{max} (Å)	90 ± 5	90 ± 5	90 ± 5	80 ± 5	80 ± 5	70
V_p (10^3 Å^3)	63 ± 6	52 ± 5	43 ± 5	35 ± 4	42 ± 5	45
MM (kDa)	44 ± 5	42 ± 5	35 ± 4	25 ± 4	22 ± 3	24.3
χ^{MDT}	2.45	1.72	1.56	1.25	-	-
χ^{MTT}	1.84	1.47	1.41	1.17	-	-
χ^{MDTT}	1.84	1.43	1.35	1.15	1.45	-
V_{mon} (%)	0	0	6 ± 5	24 ± 5	0	-
V_{dim} (%)	0	8 ± 5	25 ± 5	24 ± 5	100	-
V_{tri} (%)	48 ± 5	47 ± 5	54 ± 5	52 ± 5	0	-
V_{tet} (%)	52 ± 5	45 ± 5	15 ± 5	0	0	-

[a] Notations: R_g, radius of gyration; D_{max}, maximum size; V_p, excluded volume of the hydrated particle; MM, molecular mass of the solute; χ, discrepancy between the expetimental data and best fits from mixtures (χ^{MDT}, monomers/dimers/tetramers; χ^{MTT}, monomers/trimers/tetramers; and χ^{MDTT}, monomers/dimers/trimers/tetramers); V_{mon}, V_{dim}, V_{tri}, and V_{tetr}, volume fractions of the oligomeric species for the latter fits. The rightmost column gives the values computed from the NMR model.

From the previous amide proton R_1 measurement of free Adx, it was found that PRE is insignificant when the atom is more than 16 Å away from the 2Fe−2S cluster.[31] Therefore, the intermolecular PREs observed for C*c* residues were converted to lose distance restraints (10−20 Å). A total of 100 structures with the lowest energies was selected for further refinement. In the last refinement stage, the extra energy term defining the geometry of disulfide bond[32] was added. The final ensemble of the 10 best structures and restraints used for structure modeling has been submitted to the PDB, entry 2JQR.

PCS Simulations. The structure coordinates of C*c* (PDB entry 1YCC) and Adx (PDB entry 1AYF) were used for PCS simulations. The relative diffusional movement of the proteins in the native complex was decomposed into two types of rotations. One is the rotation of Adx around its own center of mass (wobbling motion), and the other is the rotation of Adx around the C*c*, resulting in the translational movement over its surface. It should be noted that from the point of view of Adx, the former can be considered as rotation of C*c* around Adx and the second as wobbling of C*c*. For the convenience of calculation, the heme metal center of C*c* was used as the rotating center for the second movement. Pseudo-atoms representing the magnetic susceptibility tensor were used as the reference frame. Each rotation can be further decomposed into the rotations around the *X*, *Y*, and *Z* axes. Six angle variables are thus used to describe the rotation range. The initial orientation of two proteins was generated in a way that N16 of C*c* is in close contact with L80 of Adx. The initial distance of two rotating centers was set to be 29 Å. This brings the proteins together in an orientation with the centers of the CSP affected areas at close distance. Then, the effect of averaging over the six rotating and wobbling axes was evaluated by generating 40−200 orientations randomly within a given angle range. If the rotation caused the structures in a certain orientation to be either clashing or not touching, the distance was increased or decreased until both proteins were just in contact. The averaged intermolecular PCSs were calculated for amide protons of Adx in this ensemble and compared to the PCSs predicted for the starting structure. The significance cutoff of proton PCS was set to be 0.025 ppm. The rotations of Adx around C*c* in the direction that changes the angle between Adx and the heme plane (θ) lead to the most averaging of the PCS. On the other hand, rotations of Adx around its center of mass (wobbling) have a smaller effect. The CSP map of C*c* shows effects mostly at the front face[3] around the heme edge, implying that the angle range for Adx rotation is small. It was estimated to be at most $\theta = 75°$. The angles for Adx wobbling need to be at least 100−120° to reduce the PCS to below the detection limit.

Results

Heterodimer Formed by CcV28C and AdxL80C. To study the degree of dynamics in the complex of C*c* and Adx, a comparison was made between the native complex and a CL counterpart. The proteins were cross-linked by using a disulfide bridge between engineered cysteine residues on C*c* (V28C) and the truncated form of Adx (residues 4-08,[22] mutant L80C; in the following text, Adx refers to Adx4-108). The cysteine mutants were designed on the basis of previous chemical-shift mapping data[3] such that they are exposed on the surfaces and close to the predominant interaction interface. The CL complex does not necessarily mimic the ET active form but should represent a well-defined complex that is much less mobile than the native complex. Cross-linking experiments show that C*c*V28C and AdxL80C mutants can be linked by a disulfide bond with the best yield (20−30%) under high ionic strength conditions. The CL products were separated by using ion-exchange chromatography. Analytical gel filtration shows that the engineered heterodimer has a molecular weight about 20−30 kDa (expected 23.5 kDa). The heterodimer of ^{15}N-C*c*V28C and AdxL80C was also characterized by mass spectrometry, which confirmed the formation of the heterodimer (data not shown).

SAXS. SAXS was employed to analyze the oligomeric composition of C*c*/Adx complexes in solution. In 10 mM Hepes buffer, pH 7.4, the overall parameters of the CL complex in Table 1 indicate that it remains heterodimeric at all solute concentrations, independent of the presence of NaCl. The low resolution shapes of the complex reconstructed from the SAXS data ab initio and by rigid-body analysis (Figure 1A and Supporting Information, Figure S4, curve 1) match the NMR-predicted model (see below, Structural Modeling of CL Complex). The native complex demonstrates a completely different behavior, strongly depending on the solute concentration and ionic strength in 10 mM Hepes buffer. The experimental curve at 200 mM NaCl can be fitted well by the computed scattering from a mixture of C*c* and Adx (Supporting Information, Figure S1, curve 2), indicating that the native complex is an electrostatic complex and dissociates at higher NaCl concentrations. A reduction in salt concentration promotes formation of dimeric species, but also higher oligomers are observed (see more detail in Supporting Information, Table S2). In salt-free solutions with low protein concentration (2.4 mg/mL), the

(31) Beilke, D.; Weiss, R.; Löhr, F.; Pristovsek, P.; Hannemann, F.; Bernhardt, R.; Rüterjans, H. *Biochemistry* **2002**, *41*, 7969–7978.
(32) Petersen, M. T. N.; Jonson, P. H.; Petersen, S. B. *Protein Eng.* **1999**, *12*, 535–548.

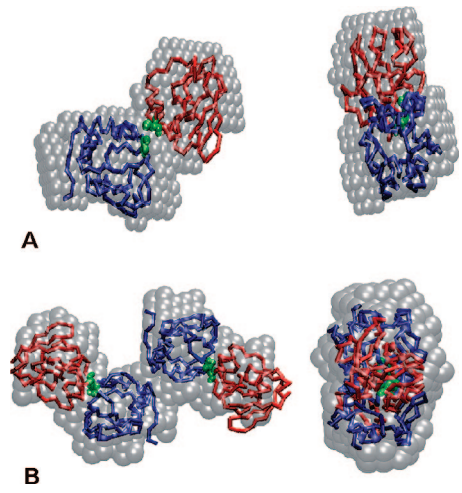

Figure 1. Ab initio bead model of CL complex and native tetramer model obtained from SAXS data. (A) Ab initio bead model of CL complex obtained by DAMMIN (gray semitransparent spheres) superimposed with the rigid-body model of the heterodimer constructed by SASREF. The C*c* and Adx models are displayed as blue and red C_α traces, respectively. Residues Val28 of C*c* and Leu80 of Adx are indicated by green spheres. The right view is rotated counter-clockwise around the vertical axis. (B) Ab initio bead model of native complex at high concentration in salt-free buffer superimposed with the heterotetramer constructed by rigid-body refinement. The representations and color codes are the same as those in panel A.

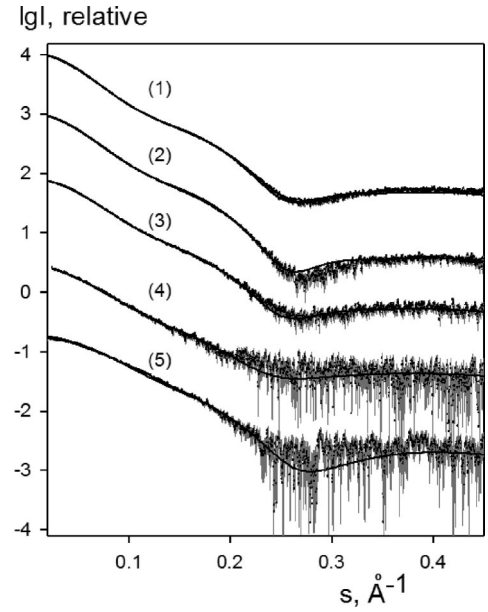

Figure 2. SAXS data from native C*c*/Adx complex in salt-free solutions. Curves 1−4 correspond to solute concentrations 24, 12, 6, and 2.4 mg/mL in 10 mM Hepes buffer, pH 7.4, respectively. Curve 5 is from 2.4 mg/mL in 20 mM potassium phosphate, pH 7.4, buffer. Dots with error bars, experimental data; solid lines, best fits by OLIGOMER from mixtures of monomers, heterodimers, trimers, and tetramers with volume fractions in Table 1, for curves 1−4. For curve 5, the best fit comes from 1:1 complex. The intensities are displayed as function of the momentum transfer $s = (4\pi \sin\theta)/\lambda$, where 2θ is the scattering angle, and $\lambda = 1.5$ Å is the X-ray wavelength, and successive curves are displaced down by one logarithmic unit for clarity.

overall parameters are close to those of a heterodimeric complex (Table 1). The size of the complex increases with protein concentration (Table 1), and at 24 mg/mL, the solute is largely tetrameric, as also revealed by ab initio and rigid-body models displaying side-by-side dimers (Figure 1B). To obtain quantitative estimates of the equilibrium, the data were fitted allowing for mixtures of different oligomers of C*c* and Adx. The analysis included monomers, heterodimers, and tetramers, but also tentative trimers built by removing one monomer from the tetramer, and these mixtures indeed provided good fits to the experimental data at different solute concentrations (Figure 2, curves 1−4). Strikingly, a significant proportion of trimeric species was detected for all concentrations, and attempts to fit the data without trimers significantly worsened the fits (Table 1). The formation of tetramers is thus proceeding via trimers and not by association of two heterodimers. The latter association would have been expected for the case of specific dimerization and teteramerization, whereas the actually observed oligomerization suggests a stochastic encounter complex formation. This finding is further corroborated by the fact that the CL heterodimer does not form tetramers even at high solute concentrations. Apparently, the CL heterodimers lack the mobility in solution necessary for the effective formation of interdomain links via an encounter mechanism.

In 20 mM potassium phosphate, pH 7.4, which is the buffer used in previous and current NMR experiments, the SAXS data indicate that the data for the native complex at 2.4 mg/mL can be well fitted with a 1:1 complex (Figure 2, curve 5, $\chi = 1.41$) or a mixture of monomers and 1:1 complex ($\chi = 1.26$); in the latter case, the volume fraction of monomeric species does not exceed 40%. At high protein concentration and a 2:1 ratio *Cc*:Adx, the curve can be fitted with a 1:1 ($\chi = 1.52$) or a mixture of 1:1 and 2:1 complexes ($\chi = 1.15$). These results indicate that the presence of 20 mM phosphate buffer largely precludes oligomerization of the complex.

CSP. Complex formation leads to changes of the chemical environment of residues in the interface because of solvation changes and interactions between the partner proteins. The resulting CSPs can be used to identify the residues involved in binding. Previously, we reported such CSPs for the formation of the native 1:1 complex of C*c* and Adx in 20 mM phosphate buffer.[3] For C*c*, the maximum chemical-shift change ($\Delta\delta_{avg}$) is only 0.08 ppm, and for Adx, the chemical-shift change is even smaller ($\leq$0.04 ppm). According to the perturbations, the dominant binding site in C*c* is around the heme edge, whereas for Adx, the effects are spread over an extensive area (Figure 3). Under the same experimental conditions, the CL complex shows perturbations with larger $\Delta\delta_{avg}$ values of up to 0.35 and 0.27 ppm for C*c* and Adx, respectively, and the residues involved are localized to the area around the site of cross-linking (Figure 3). It was proposed that in the native complex, C*c* may sample large surface area of Adx, and multiple orientations are in fast exchange. The comparison of CSP data for native and CL complex suggests that because of the disulfide bonding, reduced mobility in the single-orientation CL complex leads to a more localized interface and larger CSPs.

Intermolecular PRE. The FeS cluster in Adx is paramagnetic, causing increased relaxation and thus line broadening of the NMR resonances of nearby nuclei because of a dipolar interaction with the unpaired electrons. Not only residues of Adx are affected, also C*c* residues that get sufficiently close to the FeS cluster should experience such effects. These intermolecular paramagnetic effects should affect the transverse relaxation rates (R_2) of the protons most strongly. However, transverse relaxation is also very sensitive to the increase of the tumbling time of C*c* upon complex formation as well as exchange broadening. No diamagnetic control for the paramagnetic Adx is available to correct these effects. For this reason, the longitudinal relaxation rates (R_1) of amide protons were measured for free C*c*, C*c* in

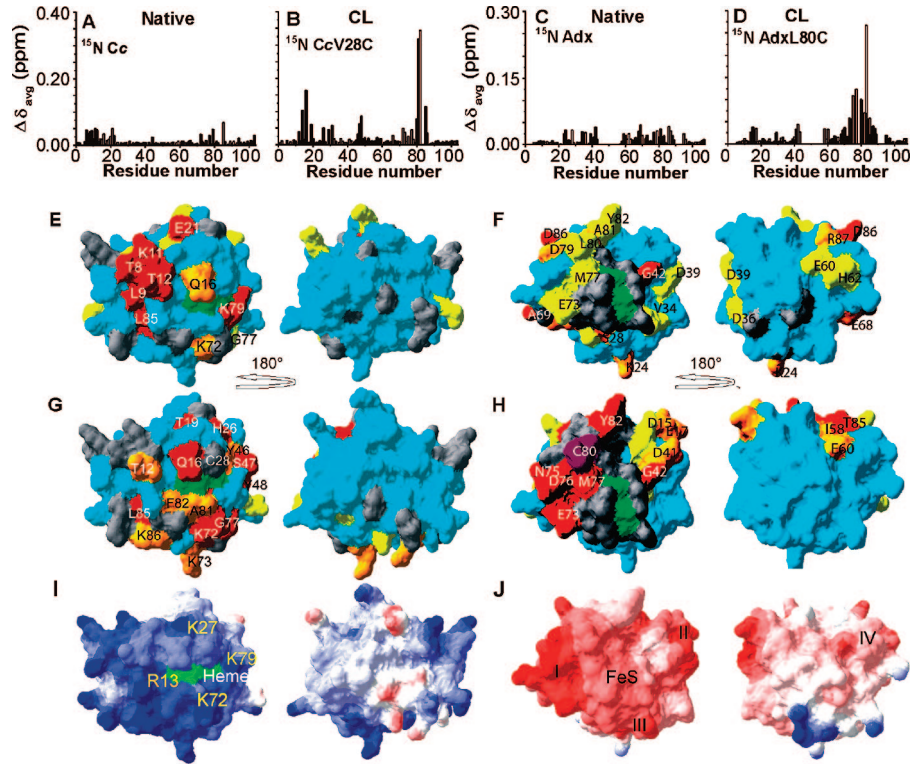

Figure 3. CSPs of native and CL complex and comparison with the electrostatic potential of C*c* and Adx (A−D) $\Delta\delta_{avg}$ for observed residues of C*c* (A, B) and Adx (C, D) for the native (A, C) and CL (B, D) complexes. CSP for the native complex were taken from literature.[3] (E−H) Surface representations of C*c* (E, G) and Adx (F, H) showing the CSP for native (E, F) and CL (G, H) complexes. Residues are colored in red, orange, yellow, and blue according to the $\Delta\delta_{avg}$ categories ($\geq$0.04, $\geq$0.03, $\geq$0.02, and <0.02 ppm, respectively). Residues without assignment are in gray, and iron sulfur binding loop and heme group are in green. (I, J) Surface representation of the electrostatic potential of C*c* (I) and Adx (J), important charged residues (R13, K27, K72, and K79 of C*c*) or patches involved (I, II, III, and IV of Adx) in the interaction are labeled.

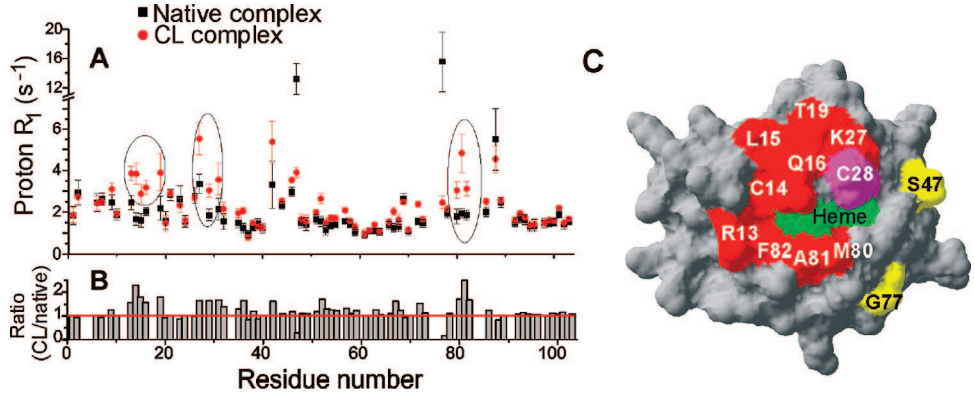

Figure 4. PRE. (A) Amide proton R_1 values are plotted for observed C*c* residues for the native (black) and CL (red) complex. (B) The ratios of R_1 values (CL/native) are plotted for observed C*c* residues. (C) Surface representation of C*c* with the site of cross-linking (C28) in magenta, residues with a R_1 ratio >1.3 in red and <0.5 in yellow, and the heme in green.

the native complex, and C*c* in the CL complex. The rates in the native-complex state are only slightly larger than those in the free state (Supporting Information, Table S4). Comparison of C*c* R_1 values in the native and CL complex indicates significant relaxation enhancement for some residues on C*c* when the orientation of the proteins has been fixed by cross-linking (Figure 4A, B). Surprisingly, two residues, S47 and G77, with large R_1 values in the free C*c* and the native complex exhibit reduced relaxation rates in the CL complex. These residues are located close to the interaction interface but on one side of C28 (marked in yellow in Figure 4C) and are relatively far from the FeS cluster. A plausible explanation is that complex formation results in protection of these amide protons from solvent exchange, bringing the R_1 values into the usual range. All other affected residues are located close to the site of cross-linking (Figure 4C), suggesting that the relaxation enhancement is attributable to the proximity of the FeS cluster, as expected for a rigid complex. The absence of significant PREs in the native complex indicates that the average distance of all C*c* protons to the FeS cluster is too large to affect R_1, in accord with a dynamic nature of the complex.

Site-Specific Spin Labeling. To explore the interaction interface on Adx, a paramagnetic spin label, MTSL, was attached to C28 of the C*c* mutant, and relaxation enhancement was measured for Adx amide protons in the native complex. C*c*V28C labeled with a diamagnetic control, MTS, was used to correct

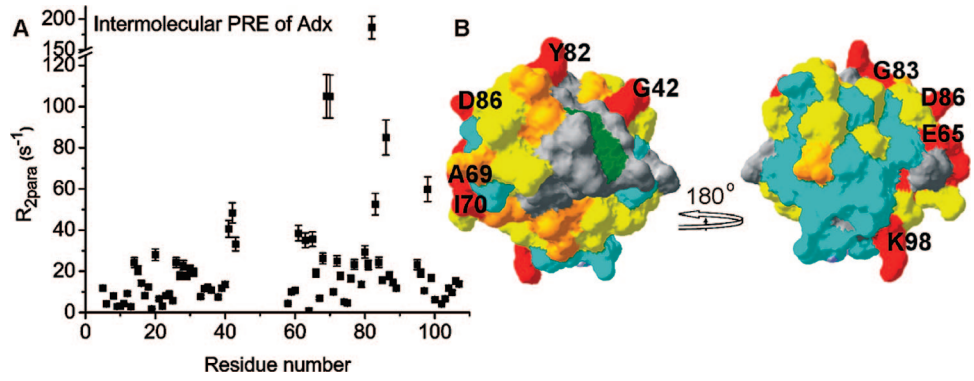

Figure 5. Spin-labeling and intermolecular PRE. (A) Relaxation enhancement $R_{2,para}$ values are plotted for observed residues of Adx complexed with spin-labeled C*c*. (B) Surface representation of Adx, showing the residues affected by a spin label attached to C*c*V28C in the native complex. Residues are colored according to $R_{2,para}$ (≥30, red; 20−30, orange; 11−20, yellow; and <10 s^{-1}, light blue). Unobserved residues are in gray, and the FeS binding loop is in green.

for all nonparamagnetic contributions to the transverse relaxation rate. The CSPs observed for Adx upon complex formation with the control-labeled C*c* are very similar to those of the native complex formed by WT C*c* and Adx, which indicates that the label does not interfere with the interaction between the proteins. In the complex with spin-labeled C*c*, many residues of Adx exhibit line broadening due to PRE. The intensity (*I*) attenuation (I_{para}/I_{dia}, Supporting Information, Table S5) was used to calculate PREs, $R_{2,para}$ (Figure 5A). A map of intermolecular PREs onto the surface of Adx (Figure 5B) shows that the residues with large $R_{2,para}$ (>30 s^{-1}, red in Figure 5B) cover half of the surface area of Adx, without forming a single localized patch. The result indicates that within the native complex, C*c* samples a large part of the surface of Adx.

Intermolecular PCS. Ferrous C*c* is diamagnetic, whereas ferric C*c* carries a single unpaired electron, giving rise to PCS of the surrounding nuclei. For most residues of C*c*, the difference in chemical shift between the oxidized and reduced state is dominated by the PCS. Upon complex formation, intermolecular PCSs are expected also for Adx nuclei, as has been reported for example in the complex of cytochrome *f* and plastocyanin.[33] By comparison of the chemical-shift changes observed for Adx binding to either ferrous or ferric C*c*, the PCS can be obtained, provided that the perturbations caused by binding are the same in both redox states. In the native complex, the chemical shifts of Adx interacting with ferric and ferrous C*c* are very similar (Figure 6A), indicating the absence of significant intermolecular PCS. In contrast, in the CL complex, chemical-shift differences are detected in some regions of Adx (Figure 6B). The shifts of the amides of residues D41-F43, I58-E60, F64, and T85-R89 show similar sizes (in ppm) and signs for amide proton and nitrogen dimensions, which is characteristic for PCS. The comparison of intermolecular PCS for native and CL complex suggests that the averaging of PCS in the native complex results from the interprotein dynamics.

PCS Simulations. The observation that Adx experiences intermolecular PCS from the heme in C*c* only in the CL but not in the native complex strongly suggests that in the latter case, such shifts are averaged by mobility of the Adx relative to C*c*. The size and sign of the PCS depends on both the metal-to-nucleus distance and the position of the nucleus within the frame of the magnetic susceptibility tensor, and thus, reduction

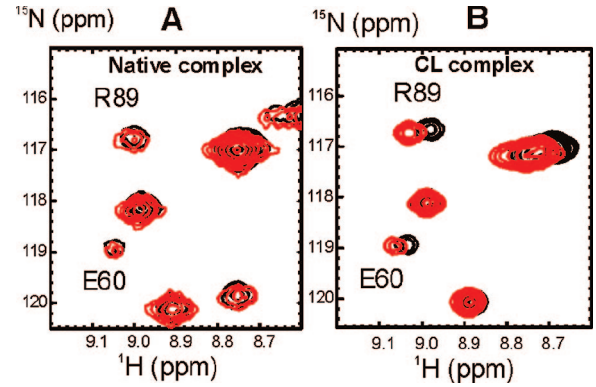

Figure 6. Intermolecular PCS detected on Adx for the native (A) and CL (B) complex. Overlays of a region of the HSQC spectra of the complexes containing ^{15}N-Adx and reduced (red) or oxidized (black) C*c* are shown.

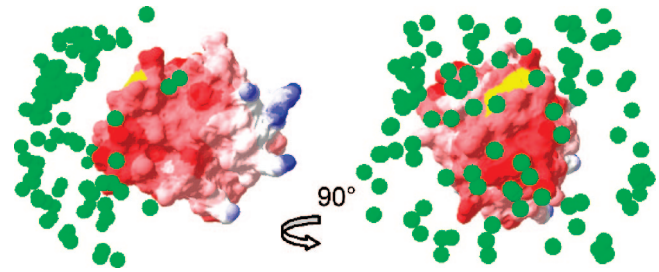

Figure 7. The ensemble of complex structures from the PCS simulation illustrates the degree of dynamics. Adx molecules are shown in surface representation colored according to the electrostatic potential with red for negative and blue for positive. The FeS binding loop is in yellow. The centers of mass of C*c* are represented by green spheres.

of the PCS can occur when Adx samples different orientations within the native complex. Simulations were carried out to determine the minimum degree of mobility of Adx that is necessary to reduce the PCS to below the detection limit. Details are given in the Materials and Methods section. Figure 7 shows the result of the simulation. C*c* positions are represented by the centers of mass and illustrate the minimum mobility required in the native complex. Clearly, C*c* needs to sample a large area on Adx. This conclusion is in accord with the extensive CSP and PRE map observed for Adx in the native complex (Figures 3 and 4).

Structural Modeling of CL Complex. The PREs and PCSs observed in the CL complex were used to determine the relative orientations of C*c* and Adx. The model of the structure was

(33) Ubbink, M.; Ejdebäck, M.; Karlsson, B. G.; Bendall, D. S. *Structure* **1998**, *6*, 323–335.

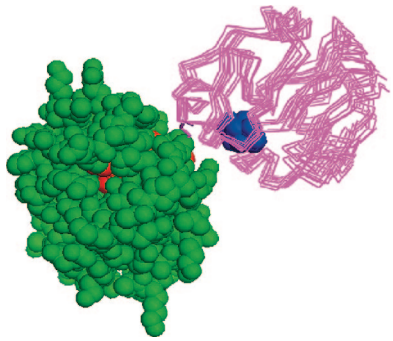

Figure 8. Structure of CL complex. The best 10 structures (rmsd 1.7 Å) are shown with the C*c* molecule superimposed in spacefilling in green with heme in red, Adx as backbone trace in magenta, and the FeS cluster in spacefilling in blue.

derived by systematic search of the conformational space assuming rigid bodies for both proteins, with free rotation around the five torsion angles that link C*c*V28C C_α to AdxL80C C_α. The structures were scored on the basis of van der Waals, PCS, and PRE energy terms. The final ensemble of 10 structures (Figure 8) has an average rmsd of 1.7 Å from the mean for the Adx heavy atoms, after superposition of the C*c* molecules. The convergence of the structure model confirmed that the CL complex exists as rigid complex. It shows that the contact surface for the CL complex contains part of the heme edge region of C*c* and the FeS loop and residues D72-Y82 of Adx. The interface in the calculated structure of the CL complex is consistent with the chemical-shift mapping. The SAXS patterns computed from the ensemble of models display a good agreement with the experimental scattering from the CL complex in solution (Supporting Information, Figure S4).

Discussion

The minimal model for protein-complex formation consists of two steps. First, the proteins form an encounter complex, in which the partners can assume multiple orientations. Then, the final, well-defined, and active complex is formed. The encounter state can be envisaged as a dynamic state, with one protein rolling over the surface of the other. Electrostatic forces are expected to dominate the interaction[34] because of their long-range effects, whereas desolvation of the protein surface is probably limited. In the classical view, the encounter state exists only briefly and proceeds quickly to the final complex. However, evidence is accumulating that the encounter state may be populated significantly in weak protein complexes. Theoretical approaches, such Brownian dynamics calculations on the ET complex of C*c* peroxidase and C*c*, suggested already decades ago that complexes can be partly of dynamic nature.[35] Experimental studies, such as fluorescence measurements on frozen solutions, supported this view.[36] Over recent years, our NMR analyses demonstrated that the average CSPs upon complex formation vary by more than 20-fold among a range of ET complexes.[37] It was proposed that the complexes which show large CSPs are predominantly in a well-defined state, whereas those with overall small perturbations are dominated by the encounter state.[37,38] This idea is rationalized by the assumption that in the encounter state, the proteins are still largely solvated, which means that the chemical environment and thus the chemical shift of the amides are hardly perturbed. The CSP caused by any specific interactions that an amide experiences in a particular conformation is averaged with all other conformations of the encounter ensemble in which that amide has no specific interaction. Also this will reduce the observed CSP. Independently, kinetic studies also showed that some weak ET complexes often should be represented by a dynamic ensemble rather than by a single complex.[5,39] The current study provides direct evidence that a protein complex can be truly dynamic and thus can be considered to represent only the encounter complex. The very nature of this state makes it difficult to characterize the complex because of the dynamics and the absence of strong interactions. Therefore, a CL counterpart of the complex was used for direct comparison. SAXS is a powerful method to probe the arrangement of domains in multiple-domain complexes, protein oligomerization, and complex formation and can provide the low-resolution molecular envelope structure of proteins or protein complexes. A few SAXS studies on redox complexes were reported previously, providing information complementary to X-ray crystallography[40,41] and solution-NMR studies.[42] Here, it was observed that only the native complex, not the CL complex, exhibits oligomerization at low ionic strength and high protein concentration. The complexes do not associate directly into tetramers, but oligomerization rather proceeds via trimers. Both observations suggest a stochastic way of association in support of a dynamic nature of the complex.

NMR CSPs were more localized and up to 6-fold larger for Adx in the CL complex as compared to the native complex, in line with the observations for other complexes mentioned above. PCSs from the heme onto Adx were observed in the CL complex, whereas they were absent in the native complex. The correlation between a dynamic complex and the absence of intermolecular PCS was first proposed for the complex formed by plastocyanin and C*c*[2] and later also for other complexes.[3,37,43] Our simulations show that C*c* has to sample a large area on Adx to reduce the intermolecular PCS to insignificant values, which is in line with the large area of interaction identified by the CSPs.

Similarly, the intermolecular PREs caused by the FeS cluster that can be observed for C*c* amides in the CL complex are absent in the native complex. Relaxation effects depend on the 6th power of the distance between the FeS cluster and the observed

(34) Suh, J. Y.; Tang, C.; Clore, G. M. *J. Am. Chem. Soc.* **2007**, *129*, 12954–12955.
(35) Northrup, S. H.; Boles, J. O.; Reynolds, J. C. L. *Science* **1988**, *241*, 67–70.
(36) McLendon, G.; Zhang, Q.; Wallin, S. A.; Miller, R. M.; Billstone, V.; Spears, K. G.; Hoffman, B. M. *J. Am. Chem. Soc.* **1993**, *115*, 3665–3669.
(37) Worrall, J. A. R.; Liu, Y. J.; Crowley, P. B.; Nocek, J. M.; Hoffman, B. M.; Ubbink, M. *Biochemistry* **2002**, *41*, 11721–11730.
(38) Prudêncio, M.; Ubbink, M. *J. Mol. Recognit.* **2004**, *17*, 524–539.
(39) Furukawa, Y.; Matsuda, F.; Ishimori, K.; Morishima, I. *J. Am. Chem. Soc.* **2002**, *124*, 4008–4019.
(40) Jones, M.; Basran, J.; Sutcliffe, M. J.; Grossmann, J. G.; Scrutton, N. S. *J. Biol. Chem.* **2000**, *275*, 21349–21354.
(41) Leys, D.; Basran, J.; Talfournier, F.; Sutcliffe, M. J.; Scrutton, N. S. *Nat. Struct. Biol.* **2003**, *10*, 219–225.
(42) Perry, A.; Tambyrajah, W.; Grossmann, J. G.; Lian, L. Y.; Scrutton, N. S. *Biochemistry* **2004**, *43*, 3167–3182.
(43) Volkov, A. N.; Ferrari, D.; Worrall, J. A. R.; Bonvin, A. M. J. J.; Ubbink, M. *Protein Sci.* **2005**, *14*, 799–811.
(44) Iwahara, J.; Clore, G. M. *Nature* **2006**, *440*, 1227–1230.
(45) Blundell, T. L.; Fernández-Recio, J. *Nature* **2006**, *444*, 279–280.
(46) Geren, L. M.; Millett, F. *J. Biol. Chem.* **1981**, *256*, 4851–4855.
(47) Müller, J. J.; Lapko, A.; Ruckpaul, K.; Heinemann, U. *Biophys. Chem.* **2003**, *100*, 281–292.

amide proton and are relatively small because the cluster is buried within Adx. In the dynamic native complex, the average distance between the amide protons of C*c* and the cluster is too large to result in PREs.

Recently, several studies showed that site-specific spin labeling combined with intermolecular PRE detection make it possible to obtain more information on low affinity, transient, and dynamic protein−DNA or protein−protein complexes by NMR.[6,7,44,45] In our case, spin labeling on an exposed residue of C*c* close to the binding interface does result in PREs of many Adx amide protons. When the amide protons come sufficiently close to the spin label, even only for a small fraction of the time, they will exhibit enhanced relaxation. Therefore, this result provides strong evidence that C*c* samples about 50% of the surface area of Adx.

A comparison of the CSP maps with the electrostatic surface potential of Adx and C*c* (Figure 3) clearly supports the notion that the encounter state is dominated by electrostatic forces. The interaction surface on Adc for C*c* comprises all four acidic patches (I−IV), whereas on C*c*, the positively charged area around the heme edge is involved in the interaction. These findings are in line with our SAXS data as well as earlier cross-linking studies between horse C*c* and Adx, which showed that Arg13 (Lys14 in horse C*c*), Lys27, Lys72, and Lys79 are involved in the interaction with Adx.[46] A docking study of horse C*c* and bovine Adx also supported this view.[47]

Conclusions

In conclusion, all the data support the view that the complex between C*c* and Adx exists as a dynamic ensemble of orientations, without a dominant, well-defined form. Thus, this complex can be taken to represent a pure encounter complex. Such a model can be used to obtain better understanding of this elusive state of interacting proteins, yielding a more comprehensive picture of the process of complex formation.

Acknowledgment. Financial support was provided by the Fonds der chem. Industrie (R.B.), the Volkswagenstiftung (R.B., M.U., and X.X., grant I/80 854), and The Netherlands Organisation for Scientific Research (M.U. and X.X., grants 700.50.026 and 700.52.425). D.S. and P.K. acknowledge support from the EU Design Study SAXIER, contract RIDS no. 011934. M.U. acknowledges the travelling grant by European Community−Research Infrastructure Action under the FP6 Structuring the European Research Area Programme (contract number: RII3-CT-2004-506008).

Supporting Information Available: Text description of the protocol for C*c*V28C ^{15}N enrichment and the SAXS analysis; five tables with SAXS data, NMR assignments, R_1 values, spin-label results, and magnetic susceptibility tensor values; four figures with SAXS results, PCS fittings, and PREs caused by TEMPOL. This material is available free of charge via the Internet at http://pubs.acs.org.

JA7101357